

# Electron spin relaxation and $^{39}\text{K}$ pulsed ENDOR studies on $\text{Cr}^{5+}$ -doped $\text{K}_3\text{NbO}_8$ at 9.7 and 240 GHz

S. Nellutla, G. W. Morley,<sup>\*</sup> and J. van Tol<sup>†</sup>*Center for Interdisciplinary Magnetic Resonance, National High Magnetic Field Laboratory, Florida State University, Tallahassee, Florida 32310, USA*

M. Pati and N. S. Dalal

*Department of Chemistry and Biochemistry, Florida State University and NHMFL, Tallahassee, Florida 32306, USA*

(Received 17 April 2008; revised manuscript received 13 June 2008; published 19 August 2008)

$\text{Cr}^{5+}$ -doped  $\text{K}_3\text{NbO}_8$ , considered to be useful as an electron spin qubit, has been investigated by pulsed  $X$  band ( $\sim 9.7$  GHz) and 240 GHz electron paramagnetic resonance and electron nuclear double resonance (ENDOR). Comparison of the low temperature electronic spin-lattice relaxation rate  $1/T_1$  at 9.7 and 240 GHz shows that it is 250 times faster at 240 GHz than at  $X$  band. On the other hand, spin-spin relaxation rate  $1/T_2$  appears largely frequency independent and is very likely related to the superhyperfine (SHF) coupling of the  $\text{Cr}^{5+}$  electron with the surrounding potassium and niobium nuclei. This coupling was investigated by hyperfine sublevel correlation spectroscopy at 9.7 GHz and pulsed Mims ENDOR at 240 GHz. The use of high frequency and field enabled us to unambiguously measure the hyperfine and quadrupole couplings of the  $^{39}\text{K}$  in spite of its small magnetic moment. We find that the largest  $^{39}\text{K}$  SHF coupling is positive, with 0.522 and 0.20 MHz as its isotropic and dipolar parts, respectively.  $^{93}\text{Nb}$  ENDOR was dominantly due to its quadrupolar interaction with a coupling of about 0.8 MHz and a SHF coupling of about 0.08 MHz. The significance of these data to spin qubit studies is pointed out.

DOI: [10.1103/PhysRevB.78.054426](https://doi.org/10.1103/PhysRevB.78.054426)

PACS number(s): 76.70.Dx, 76.30.-v, 76.60.Es, 31.30.Gs

## I. INTRODUCTION

The  $\text{Cr}^{5+}$  ion diluted in the diamagnetic host  $\text{K}_3\text{NbO}_8$  (henceforth noted as  $\text{Cr}:\text{K}_3\text{NbO}_8$ ) has been suggested as a magnetic field calibration standard for high-field electron paramagnetic resonance (EPR) experiments.<sup>1</sup> This  $S=1/2$  system exhibits a small linewidth ( $\sim 0.15$ – $0.2$  mT depending on the orientation) and the  $g$  value just below the free-electron  $g$  value,  $g_e$ . The  $I=0$  ( $^{50,52,54}\text{Cr}$ ) isotopes give rise to a single line that serves as a  $g$  marker, while the  $^{53}\text{Cr}$  (9.5%  $I=3/2$ ) yields four hyperfine lines that can be used to calibrate the linearity of the field.<sup>1</sup>

Recently  $\text{Cr}:\text{K}_3\text{NbO}_8$  has also been suggested<sup>2</sup> as a transition metal ion based single electron spin qubit system for quantum information processing. Quantum computation requires, among others, a long spin-lattice relaxation time  $T_1$  as well as a long spin-spin or spin-memory relaxation time  $T_2$ . The latter time provides a measure of the decoherence processes in the material and is used to calculate the figure of merit of a qubit, which is defined as the number of operations that can be performed before the phase information is lost. On the other hand, a “reset” of the qubit to a well-defined starting state takes a time proportional to  $T_1$ . Hence, shorter  $T_1$  time means enhanced computing speed. It is therefore desirable to understand the  $T_1$  and  $T_2$  relaxation processes via their temperature and frequency dependence.

The present work reports on our detailed measurements of the electronic  $T_1$  and  $T_2$  relaxation processes in  $\text{Cr}:\text{K}_3\text{NbO}_8$  from ambient temperatures down to 4 K at  $X$  band ( $\sim 9.7$  GHz,  $\sim 0.35$  T) and at 240 GHz ( $\sim 8.7$  T). We find that the low temperature relaxation time  $T_1$  is strongly frequency dependent: it decreases by a factor of 250 on going from 9.7 to 240 GHz. On the other hand,  $T_2$  was found to be

frequency independent in the investigated temperature range.

In order to understand the process(es) controlling the  $T_2$  we first employed hyperfine sublevel correlation (HYSCORE) spectroscopy<sup>3</sup> at  $X$  band and found that the nuclei responsible for  $T_2$  are the neighboring  $^{39}\text{K}$  nuclei. However the magnitudes of  $^{39}\text{K}$  Zeeman, superhyperfine (SHF), and quadrupole interactions are such that the analysis at  $X$  band becomes very complicated for any definitive analysis. On the other hand, the utilization of the high frequency (240 GHz) pulsed-EPR/electron nuclear double resonance (ENDOR) spectrometer yielded ENDOR peaks that could easily be assigned to the neighboring  $^{39}\text{K}$  as well as to the  $^{93}\text{Nb}$  nuclei, showing the advantage of the higher frequency/field EPR/ENDOR spectroscopy. The data clearly suggest that the  $T_2$  process, and thus also the linewidths of the continuous-wave (cw) EPR peaks, are related to the unresolved SHF coupling to the  $^{39}\text{K}$  and  $^{93}\text{Nb}$  nuclei. We note that there are only a few low frequency electron spin echo envelope modulation<sup>4</sup> and cw-ENDOR<sup>5–7</sup> studies where the  $^{39}\text{K}$  hyperfine couplings were resolved.

This paper is organized as follows. Section II provides the experimental details on the crystal structure, synthesis, EPR, and ENDOR spectrometers. The results and analysis are presented in Sec. III, and the salient points are summarized in Sec. IV.

## II. EXPERIMENTAL DETAILS

The  $\text{Cr}:\text{K}_3\text{NbO}_8$  sample was synthesized according to the published procedure.<sup>1</sup> A typical synthesis involves addition of  $\text{CrO}_3$  to a room temperature solution of  $\text{K}_3\text{NbO}_8$  and cooling to  $-15$  °C to form a 50% ice slurry followed by dropwise addition of cold 30%  $\text{H}_2\text{O}_2$ . Light yellow crystals of

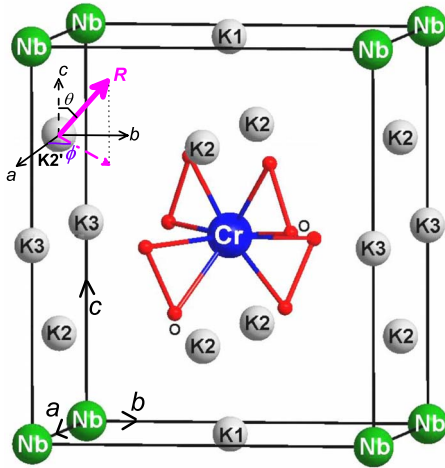


FIG. 1. (Color online) Unit cell structure of Cr:K<sub>3</sub>NbO<sub>8</sub>. Dodecahedral coordination geometry is shown only for central ion for clarity. The x, y, and z axes are along crystal a, b, and c axes, respectively. The potassium ions labeled as K2 and K2' have an appreciable overlap with Cr 3d<sub>x<sup>2</sup>-y<sup>2</sup></sub> orbital, whereas the ions labeled as K1 and K3 are in the unpaired electron nodal plane. The definitions of the angles  $\theta$  and  $\phi$  are shown by the vector  $R$  on K2'.

Cr:K<sub>3</sub>NbO<sub>8</sub> were obtained after keeping the final reaction mixture at 5 °C for two to three days. The Cr<sup>5+</sup> concentration in the studied Cr:K<sub>3</sub>NbO<sub>8</sub> samples was determined to be ~0.03 mol % by comparing its EPR signal intensity with a reference sample (BDPA:benzene complex in polystyrene, where BDPA stands for  $\alpha, \gamma$ -Bisdiphenylene- $\beta$ -phenylallyl radical) of known number of spins.

The crystal structure of Cr<sup>5+</sup>-doped K<sub>3</sub>NbO<sub>8</sub> is shown in Fig. 1. This system has a body-centered tetragonal crystal lattice ( $I\bar{4}2m$  space group) with cell parameters  $a=b=6.7862(3)$  Å,  $c=7.8312(7)$  Å, and  $\alpha=\beta=\gamma=90^\circ$ . The Cr<sup>5+</sup> ion occupies the Nb<sup>5+</sup> position and for convenience is shown at the body-center position in Fig. 1. Each Cr<sup>5+</sup>/Nb<sup>5+</sup> ion is surrounded by four peroxy (O<sub>2</sub><sup>2-</sup>) groups (shown as red balls in Fig. 1) in a dodecahedral arrangement with x, y, and z axes along crystal a, b, and c axes, respectively.

The 9.7 GHz cw- and pulsed-EPR measurements were performed on a commercial Bruker Elexsys 580 instrument with a Flexline dielectric resonator using single crystals with an approximate size of  $2 \times 1 \times 1$  mm<sup>3</sup>. The data at 240 GHz were collected on a home-built superheterodyne high field cw-EPR instrument<sup>8</sup> which is recently extended to pulsed operation.<sup>9</sup> The single crystals used were typically  $0.2 \times 0.1 \times 0.1$  mm<sup>3</sup> in size. A semiconfocal Fabry-Perot resonator was used with a 12.5 mm spherical gold-coated mirror and a semitransparent flat mirror, consisting of a gold mesh deposited on a 160  $\mu$ m thick quartz cover slip. The maximum available power at this frequency is of the order of 20 mW and the typical  $\pi/2$  pulse length is 200 ns.

The ENDOR coil for the 240 GHz spectrometer consisted of a single copper wire parallel to the mesh, which was led through a quartz capillary (0.3 or 0.25 mm outer diameter). The single crystal was attached to the outside of the quartz capillary. A typical pulse sequence for the Mims ENDOR experiment consisted of a stimulated-echo sequence<sup>11</sup> of

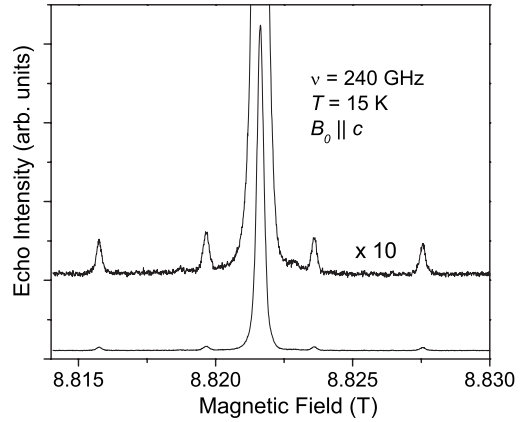


FIG. 2. Electron spin echo detected EPR spectrum at 240 GHz and 15 K for  $B_0 \parallel c$  axis. The central peak is from  $I=0$  <sup>50,52,54</sup>Cr nuclei whereas the four small peaks separated by ~4 mT are from the hyperfine coupling of the unpaired electron to <sup>53</sup>Cr nucleus (9.5%  $I=3/2$ ).

three  $\pi/2$  pulses of about 240 ns length separated by 600 ns ( $\tau$ ) and 200  $\mu$ s ( $t$ ). A 150  $\mu$ s radio frequency (rf) pulse was applied between second and third millimeter wave pulses. About 10 W of power was applied to the untuned ENDOR “coil.” The pulsed ENDOR measurements were performed at around 5–6 K. Typically 20 shots were averaged per radio frequency step and the total acquisition time of an ENDOR spectrum was of the order of 20–30 min.

### III. RESULTS AND DISCUSSION

Figure 2 shows a typical 240 GHz electron spin echo (ESE)-detected EPR spectrum obtained by measuring the integrated echo intensity after a two pulse Hahn-echo sequence<sup>11</sup> ( $\pi/2-\tau-\pi$ -echo). The ESE-EPR spectra of Cr:K<sub>3</sub>NbO<sub>8</sub> show an intense central peak from the  $I=0$  isotopes (4.34% <sup>50</sup>Cr, 83.8% <sup>52</sup>Cr, 2.36% <sup>54</sup>Cr) with a purely axial g tensor with  $g_{\parallel}=1.9472 \pm 0.0002$  for the field  $B_0 \parallel c$  and  $g_{\perp}=1.9878 \pm 0.0002$  for  $B_0 \perp c$ . The g values indicate that the  $D_{2d}$  symmetry is preserved on substitution of Nb<sup>5+</sup> with Cr<sup>5+</sup> and that the ground state is a <sup>2</sup>B<sub>1</sub> state with the unpaired electron mainly in the 3d<sub>x<sup>2</sup>-y<sup>2</sup></sub> orbital.<sup>1,2,10</sup> In the 4–300 K temperature range these g values are almost completely temperature independent.<sup>10</sup> Apparently for this CrO<sub>3</sub><sup>3-</sup> peroxy ion, which can be regarded as a heavily distorted tetrahedral system, the orbital degeneracy is sufficiently lifted for the Jahn-Teller effect to not play a role in this system. The four peaks flanking the central peak are the expected four hyperfine transitions from the  $I=3/2$  of <sup>53</sup>Cr nucleus. The hyperfine coupling also shows axial symmetry with splittings of  $3.955 \pm 0.008$  mT for  $B_0 \parallel c$  and  $1.149 \pm 0.005$  mT for  $B_0 \perp c$ . All relaxation and ENDOR measurements described below were performed on the central  $I=0$  peak.

#### A. Spin-lattice relaxation

The spin-lattice relaxation time  $T_1$  of Cr:K<sub>3</sub>NbO<sub>8</sub> at 9.7 and 240 GHz was measured by an inversion-recovery method<sup>11</sup> employing the sequences  $\pi-\tau-\pi/2$ -FID (free in-

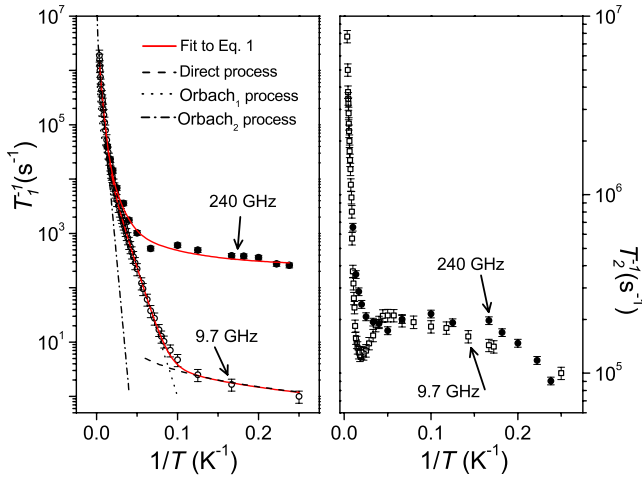


FIG. 3. (Color online) Temperature dependence of  $1/T_1$  (left panel) and  $1/T_2$  (right panel) relaxation rates at 9.7 and 240 GHz for  $B_0 \parallel c$  axis. The solid red lines in the left panel are fits to Eq. (1) with parameters listed in Table I. The individual contributions to  $1/T_1$  are also shown (see text for details).

duction decay) and  $\pi-t-\pi/2-\tau-\pi-\tau$ -echo, respectively. The left panel in Fig. 3 shows the temperature dependence of  $1/T_1$  for  $B_0 \parallel c$  at 9.7 and 240 GHz. At 9.7 GHz the  $T_1$  increases from about 500 ns at room temperature to about 1 s at 4 K. Above 25 K the  $T_1$  at 240 GHz is the same as that at 9.7 GHz but it reaches  $\sim 4$  ms at 4 K. We attempted to fit the 9.7 and 240 GHz  $T_1$  data to different models that included various combinations of (a) direct process<sup>12</sup> with  $T_1^{-1} \propto \coth(\hbar\omega/2kT)$ , (b) Raman process<sup>13</sup> with  $T_1^{-1} \propto T^{3+2m}$ , where  $m$  is the spectral dimensionality that depends on the spin system, and (c) Orbach process<sup>12</sup> with  $T_1^{-1} \propto 1/[e^{\Delta_1/kT} - 1]$ . The best fit to the data was found to be with the model given in Eq. (1),

$$T_1^{-1} = C_1 \coth(\hbar\omega/2kT) + C_2 [e^{\Delta_1/kT} - 1] + C_3 [e^{\Delta_2/kT} - 1]. \quad (1)$$

As can be seen from the solid lines in Fig. 3, the temperature dependence of the spin-lattice relaxation rate  $1/T_1$  at 9.7 and 240 GHz was successfully modeled with Eq. (1) and the best-fit parameters are listed in Table I.

It is noteworthy that the spin-lattice relaxation rate  $1/T_1$  at low temperatures (4–10 K) is considerably faster at 240 GHz

TABLE I. Fit parameters of temperature dependence of  $1/T_1$  at 9.7 GHz and 240 GHz. The values listed correspond to the solid lines in Fig. 3.

Parameter	Best-fit value	
	9.7 GHz	240 GHz
$C_1$	0.070(8) s <sup>-1</sup>	250(8) s <sup>-1</sup>
$C_2$	$6(1) \times 10^4$ s <sup>-1</sup>	$6(1) \times 10^4$ s <sup>-1</sup>
$\Delta_1$	75(3) cm <sup>-1</sup>	75(3) cm <sup>-1</sup>
$C_3$	$3.35(73) \times 10^6$ s <sup>-1</sup>	$3.35(73) \times 10^6$ s <sup>-1</sup>
$\Delta_2$	255(20) cm <sup>-1</sup>	255(20) cm <sup>-1</sup>

as compared to that at 9.7 GHz which indicates that the direct process is important at these temperatures. However, the ratio of the direct process contribution to  $1/T_1$  at 240 and 9.7 GHz is not as large as the expected  $\omega^5 \coth(\hbar\omega/2kT)$  dependence for a Kramers system<sup>12</sup> but it is closer to the  $\omega^3 \coth(\hbar\omega/2kT)$  dependence in the non-Kramers spin systems.<sup>12</sup> For example, at 4 K the observed ratio of the direct process contribution between 240 and 9.7 GHz is about 1/4 of the calculated  $\omega^3 \coth(\hbar\omega/2kT)$  value whereas it is about  $4 \times 10^{-4}$  times the  $\omega^5 \coth(\hbar\omega/2kT)$  value. This difference in the frequency dependence has been observed before<sup>14,15</sup> and needs further theoretical analysis which is beyond the scope of this undertaking.

On the other hand, the spin-lattice relaxation rate  $1/T_1$  for  $T > 10$  K at 9.7 and 240 GHz frequencies is well described (see Fig. 3) by two Orbach relaxation pathways involving thermally accessible energy levels at  $\Delta_1 \sim 75$  cm<sup>-1</sup> and  $\Delta_2 \sim 255$  cm<sup>-1</sup>. Based on the earlier infrared and Raman studies,<sup>16</sup> the 75 cm<sup>-1</sup> mode can be ascribed to the translational and librational modes, found to be below 200 cm<sup>-1</sup> in the peroxychromate ion. Similarly, the 255 cm<sup>-1</sup> mode compares with the bending vibrational modes reported in the 200–400 cm<sup>-1</sup> region in the peroxychromate ion.

## B. Spin-spin relaxation

The standard two-pulse Hahn-echo sequence was used to obtain the spin-spin relaxation time  $T_2$  at both 9.7 and 240 GHz. The right panel of Fig. 3 shows the  $1/T_2$  rate as a function of temperature for  $B_0 \parallel c$ . At 9.7 GHz the  $T_2$  increases from  $\sim 150$  ns at room temperature to  $\sim 8$   $\mu$ s at 50 K, then decreases to  $\sim 5$   $\mu$ s at 20 K, and finally increases to  $\sim 10$   $\mu$ s at 4 K. In contrast to  $T_1$ , the  $T_2$  time does not show a strong field dependence. However, the temperature dependence of  $T_2$  at both frequencies shows a minimum at about 20 K. We tentatively ascribe this minimum to some sort of motional narrowing caused by the increase in the spin fluctuations of K and Nb hyperfine fields as the temperature is raised above about 20 K. This type of temperature dependence has previously been reported for dilute solutions of free radicals<sup>17–19</sup> and other Cr<sup>5+</sup> complexes.<sup>20</sup> Above 50 K, the spin-spin relaxation time  $T_2$  is mainly governed by the spin-lattice relaxation processes.

## C. SHF interactions

As mentioned earlier the hyperfine interaction of the unpaired electron with the  $^{53}\text{Cr}$  in Cr:K<sub>3</sub>NbO<sub>8</sub> was explored previously,<sup>10</sup> and therefore in this paper we will only address the SHF coupling with the potassium ( $I=3/2$   $^{39}\text{K}$ ) and niobium ( $I=9/2$   $^{93}\text{Nb}$ ) nuclei. We believe that the electronic spin-spin relaxation processes in Cr:K<sub>3</sub>NbO<sub>8</sub> are most likely influenced by these interactions and in order to characterize them we used HYSORE spectroscopy at 9.7 GHz and pulsed Mims ENDOR at 240 GHz.

The HYSORE spectra of Cr:K<sub>3</sub>NbO<sub>8</sub> at 40 K are shown in Fig. 4 for the orientation along the  $c$  axis (bottom panel) and an orientation in the  $ab$  plane (top panel). The spin echo modulations due to the interactions with neighboring potassium nuclei are very large, which resulted in a good quality

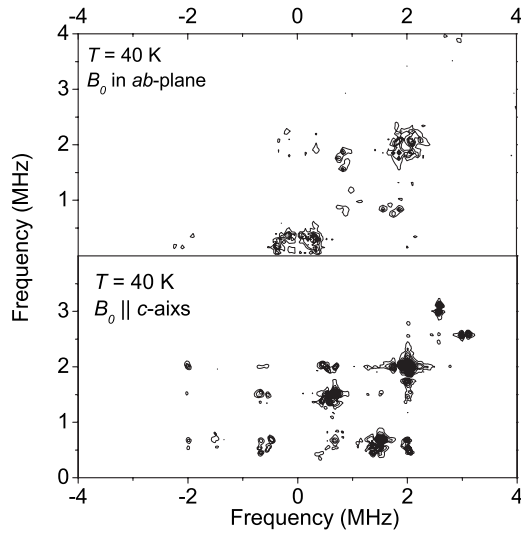


FIG. 4. HYSORE spectra of Cr:K<sub>3</sub>NbO<sub>8</sub> at 9.7 GHz and 40 K. The top panel represents  $B_0$  in the  $ab$  plane and the bottom panel for  $B_0 \parallel c$  axis.

HYSORE spectrum. However, the spectra were found to be too complex for analysis possibly because at 9.7 GHz, the Zeeman, quadrupole, and SHF interactions become comparable and lead to a complex interplay of these interactions. We therefore resorted to ENDOR measurements at 240 GHz ( $\sim 8.7$  T) where the Zeeman terms become dominant.

At 240 GHz, pulsed ENDOR signals of  $^{39}\text{K}$  were measured at various crystal orientations (see Fig. 5). A systematic study of the orientation dependence of the ENDOR could not be performed due to the unavailability of a goniometer for

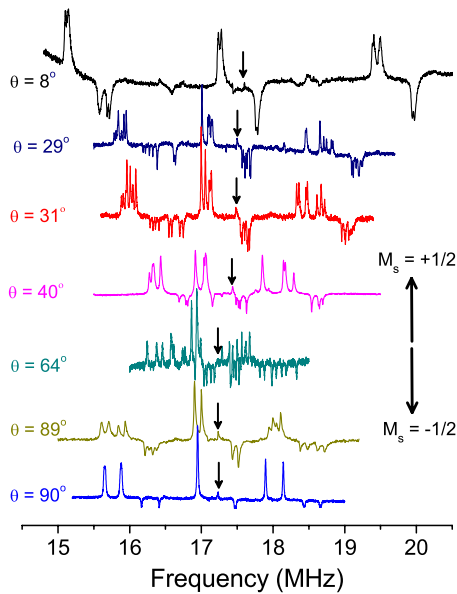


FIG. 5. (Color online) Mims ENDOR spectra of  $^{39}\text{K}$  at 240 GHz and 5 K at several crystal orientations.  $\theta$  indicates the angle between  $B_0$  and the  $c$  axis. Echo intensity increases during the ENDOR transitions in the  $M_s = +1/2$  manifold (upward peaks), while it decreases for the ENDOR transitions in the  $M_s = -1/2$  manifold (downward peaks). The arrows correspond to the nuclear Zeeman frequency of 17.25 MHz.

this spectrometer at the present time. While the angle ( $\theta$ ) of  $B_0$  relative to the crystal  $c$  axis can be accurately determined from the resonance field of the EPR transition (via the  $g$ -tensor anisotropy), the axial  $g$ -tensor symmetry does not help with the precise determination of the angle  $\phi$  of  $B_0$  in the  $ab$  plane. However, a closer look at the crystal structure (see Fig. 1) reveals that only the eight potassium nuclei labeled as K2 and K2' have an appreciable overlap with the  $\text{Cr}^{5+} 3d_{x^2-y^2}$  orbital and therefore are expected to be responsible for the  $^{39}\text{K}$  ENDOR signals. These eight equivalent nuclei are related by symmetry ( $xyz, \bar{x}yz, x\bar{y}z, \bar{x}\bar{y}z, yx\bar{z}, \bar{y}x\bar{z}, y\bar{x}\bar{z}, \bar{y}\bar{x}\bar{z}$ ), and at some orientations eight sets of signals can indeed be distinguished (e.g.,  $\theta = 31^\circ$  spectrum in Fig. 5).

It should be noted that both negative (smaller stimulated-echo) and positive (larger stimulated-echo) signals are observed and that the signal intensities are quite large. When on ENDOR resonance, the observed echo height varied from 40% to 200% of the echo height observed without rf power or out of resonance. The ENDOR intensity is largest when the shot-repetition time is of the order of  $T_1$ . This implies that the  $^{39}\text{K}$  nuclei are strongly polarized by the pulse sequence, leading to an increase in echo intensity when a nuclear transition in the  $M_s = +1/2$  electron manifold is addressed, while the echo intensity becomes smaller when a transition in the  $M_s = -1/2$  state is excited, as explained in Ref. 21. These anomalous ENDOR intensities occur when the microwave quantum ( $\hbar\omega$ ) is of the same order or larger than the thermal energy  $kT$  and allows for the determination of the sign of the hyperfine coupling in both pulsed<sup>21,22</sup> and cw-ENDOR.<sup>23</sup> The observed sets of  $^{39}\text{K}$  ENDOR signals are sufficient for a unique assignment of the SHF and quadrupole tensor values and their relative orientations. The data are analyzed by the diagonalization of the usual effective spin Hamiltonian given in Eq. (2) with  $S=1/2$  and  $I=3/2$ ,

$$\hat{H} = \mu_B \vec{B}_0 \vec{g} \hat{S} + \sum_n (\hat{S} \tilde{A}_n \hat{I}_n - \gamma_n \vec{B}_0 \hat{I}_n + \hat{I}_n \tilde{Q}_n \hat{I}_n). \quad (2)$$

Here,  $\vec{g}$  is the electron Zeeman tensor and  $\tilde{A}$  and  $\tilde{Q}$  are, respectively, SHF and quadrupole tensors of the surrounding nuclei. The principal values and their directions of the  $\tilde{A}$  tensor (namely,  $A_1, A_2, A_3$ ) and  $\tilde{Q}$  tensor (namely,  $Q_1, Q_2, Q_3$ ) for the K2' nucleus obtained from the analysis are given in Table II. The tensors for the other chemically equivalent K2 nuclei can be obtained via the aforementioned crystal symmetry operations. Use of SHF values listed in Table II yields the isotropic SHF interaction as +0.522 MHz. Comparison of this observed isotropic SHF coupling to that of the experimental hyperfine splitting (231 MHz) of atomic potassium<sup>24</sup> in the ground state or the listed theoretical value (228 MHz) in Ref. 25 indicates a spin density of 0.23% in the  $4s$  orbital.

While we cannot make a completely unambiguous assignment of the specific potassium nucleus associated with each of the eight sets of SHF and quadrupole tensors, it is natural to assume that the anisotropic contribution to the SHF interaction should reflect the dipolar interaction between the potassium nuclear spin and the chromium electron spin. We

TABLE II. The principal values and their directions of  $^{39}\text{K}$  SHF and quadrupole tensors determined by 240 GHz Mims ENDOR. These values correspond to K2' and the values for the remaining seven K2 potassium ions can be obtained from the symmetry relations given in the text.  $\theta$  is the angle with the  $c$  axis and  $\phi$  the angle in the  $ab$  plane (see Fig. 1). The errors in the directions are estimated to be  $2^\circ$ .

	Value (MHz)	$\theta$	$\phi$
$A_1$	+0.407(5)	147	90
$A_2$	+0.425(5)	90	0
$A_3$	+0.733(5)	57	90
$Q_1$	-0.423(4)	87.6	65.6
$Q_2$	-0.329(4)	90.6	-24
$Q_3$	0.752(4)	2.5	-100

therefore assign the SHF tensor given in Table II to the potassium for which the  $A_3$  direction is close to the Cr-K direction (labeled as K2' in Fig. 1).

The experimental anisotropic  $^{39}\text{K}$  superhyperfine interaction (-0.115, -0.097, and 0.211 MHz) is somewhat larger than the contribution from a simple K-Cr point-dipole approximation (-0.062, -0.062, and 0.124 MHz). This may be due to the fact that only  $\sim 90\%$  of the electron spin is on the  $3d_{x^2-y^2}$  orbital and the rest of the spin density is distributed over the  $2p$  orbitals of the oxygen ions surrounding the  $\text{Cr}^{5+}$  ion<sup>10</sup> and other ions (e.g., 1.8% on the  $4s$  orbitals of the eight K2 ions). This makes the simple point-dipole approximation inadequate. It should be noted that the nearest oxygens, the potassium ions K1 and K3, as well as the niobium ions lie in the nodal planes of the  $^2B_1$  ground state, and no spin density can be expected in  $s$  orbitals on these ions.

Alternatively, via overlap with the oxygen orbitals there may also be some spin density in the potassium  $3d$  and/or  $4p$  orbitals, although they are significantly higher in energy than the  $4s$  orbital. A contribution of 50 kHz to the anisotropic SHF splitting corresponds to spin densities in the  $3d$  and/or

$4p$  orbitals of the order 1%. At this point we cannot distinguish between these different contributions without detailed quantum chemical calculations, and a more precise analysis of the  $^{39}\text{K}$  SHF is reserved for future studies.

The quadrupole tensor of K2' is not entirely axial and has the direction of its largest principal value close to the  $c$  axis. The small deviation from the  $c$  axis indicates that the site symmetry of the  $\text{K}^+$  ions is slightly lowered. This deviation also implies that the local surrounding of the  $\text{Cr}^{5+}$  ion is slightly distorted as compared to that of the  $\text{Nb}^{5+}$  ion in the undoped lattice while preserving the  $\text{Cr}^{5+}$   $D_{2d}$  site symmetry.

At some crystal orientations  $^{93}\text{Nb}$  ( $I=9/2$ ) ENDOR is also observed. The ENDOR spectrum with the field  $40^\circ$  from the crystal  $c$  axis is shown in Fig. 6(b). We speculate that at most orientations the SHF interaction is too small to give an appreciable ENDOR intensity, but it can be detected when the field is along the Cr-Nb dipolar direction because of the largest dipolar interaction in this direction. Since  $\text{Cr}^{5+}$  and  $\text{Nb}^{5+}$  ions are fairly well separated ( $\sim 6.2$  Å), the dipolar contribution to the Cr-Nb SHF interaction can be estimated using a point dipolar approximation as  $b[3\cos^2(\psi)-1]$  with  $b\sim 0.08$  MHz and  $\psi$  as the angle between Cr-Nb dipolar axis and  $B_0$ . While the limited data prevent a detailed analysis, the  $^{93}\text{Nb}$  ENDOR spectrum in Fig. 6 can be simulated with a quadrupole tensor  $Q[3\cos^2(\theta)-1]$  with  $|Q|=0.82$  MHz under the assumption that the quadrupole tensor is nearly axial with the principal direction along the crystal  $c$  axis.

#### IV. SUMMARY

We have measured the electron spin relaxation times in Cr:  $\text{K}_3\text{NbO}_8$  using pulsed-EPR at 9.7 and 240 GHz. The SHF couplings of the electron spin with the neighboring potassium nuclei have also been determined using pulsed Mims ENDOR at 240 GHz. The ENDOR results show that the SHF interaction of the  $\text{Cr}^{5+}$  unpaired electron with neighboring potassium (labeled as K2 and K2' in Fig. 1) and the niobium nuclei is responsible for the electron spin spin relaxation  $T_2$

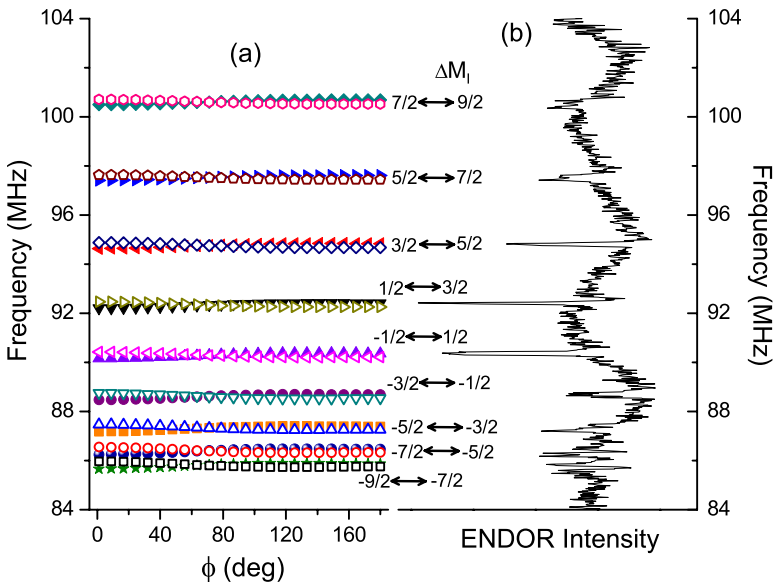


FIG. 6. (Color online) (a) Calculated energy levels as a function of  $\phi$  at 240 GHz for  $S=1/2$  and  $I=9/2$  for  $B_0$   $40^\circ$  from the  $c$  axis. Closed and open symbols shown for each  $\Delta M_I$  transition correspond to  $M_s = +1/2$  and  $-1/2$ . (b) Experimental  $^{93}\text{Nb}$  Mims ENDOR at 5 K and 240 GHz for the same orientation.

process. An unpaired spin density of about 0.2% on the K2 and K2' nuclei has been estimated from the isotropic  $^{39}\text{K}$  SHF coupling constant. While the  $T_2$  time in  $\text{Cr}:\text{K}_3\text{NbO}_8$  is largely frequency independent, its temperature dependence shows a minimum around 20 K that has been tentatively ascribed to the change in the rate of surrounding nuclear spin flip flops. At both 9.7 and 240 GHz the spin-lattice relaxation time  $T_1$  is dominated by a direct and two Orbach processes. The modes involved in the Orbach processes are assigned to bending vibrations, translational lattice vibrations, and/or libration modes of the  $\text{CrO}_8^{3-}$  ion. Furthermore, the direct process contribution to  $T_1$  at 240 GHz is found to be about more than 2 orders of magnitude larger than the contribution at 9.7 GHz. Surprisingly, the contribution ratio is closer to an  $\omega^3 \coth(\hbar\omega/2kT)$  dependence in a non-Kramers system than it is to the  $\omega^5 \coth(\hbar\omega/2kT)$  dependence expected for a

Kramers system. Further theoretical analysis is necessary to understand this divergence. Finally, the frequency dependence of relaxation times in  $\text{Cr}:\text{K}_3\text{NbO}_8$  shows that it is possible to tune  $T_1$  with the frequency/field while keeping  $T_2$  relatively the same, a feature useful in transition metal ion based spin qubits for quantum information applications.

#### ACKNOWLEDGMENTS

We thank Ronald J. Clark of the Chemistry and Biochemistry Department of the Florida State University for crystal structure determination of  $\text{K}_3\text{NbO}_8$ . S.N. and J.vT. acknowledge the State of Florida and NSF Cooperative Agreement under Grant No. DMR0654118 and NSF under Grant No. DMR0520481 for financial support. N.S.D. acknowledges NSF for funding through Grant No. DMR0506946.

\*Also at London Center for Nanotechnology, University College London, London WC1H0AH, UK.

<sup>†</sup>vantol@magnet.fsu.edu

<sup>1</sup>B. Cage, A. Weekley, L.-C. Brunel, and N. S. Dalal, *Anal. Chem.* **71**, 1951 (1999).

<sup>2</sup>S. Nellutla, K.-Y. Choi, M. Pati, J. van Tol, I. Chiorescu, and N. S. Dalal, *Phys. Rev. Lett.* **99**, 137601 (2007).

<sup>3</sup>P. Höfer, A. Grupp, G. Nebenfuehr, and M. Mehring, *Chem. Phys. Lett.* **132**, 279 (1986).

<sup>4</sup>H. Barkhuijsen, R. de Beer, A. F. Deutz, D. van Ormondt, and G. Völkel, *Solid State Commun.* **49**, 679 (1984).

<sup>5</sup>R. C. DuVarney and J. M. Spaeth, *Solid State Commun.* **32**, 1237 (1979).

<sup>6</sup>N. S. Dalal and P. K. Kahol, *Solid State Commun.* **70**, 623 (1989).

<sup>7</sup>D. Zverev, H. Vrielinck, F. Callens, P. Matthys, S. Van Doorslaer, and N. M. Khaidukov, *Phys. Chem. Chem. Phys.* **10**, 1789 (2008).

<sup>8</sup>J. van Tol, L. C. Brunel, and R. J. Wylde, *Rev. Sci. Instrum.* **76**, 074101 (2005).

<sup>9</sup>G. W. Morley, L. C. Brunel, and J. van Tol, *Rev. Sci. Instrum.* **79**, 064703 (2008).

<sup>10</sup>N. S. Dalal, J. M. Millar, M. S. Jagadeesh, and M. S. Seehra, *J. Chem. Phys.* **74**, 1916 (1981).

<sup>11</sup>A. Schweiger and G. Jeschke, *Principles of Pulse Electron Paramagnetic Resonance* (Oxford University Press, Oxford, 2001).

<sup>12</sup>A. Abragam and B. Bleaney, *Electron Paramagnetic Resonance of Transition Ions* (Clarendon, Oxford, 1970).

<sup>13</sup>B. Rakvin and N. S. Dalal, *J. Phys. Chem. Solids* **57**, 1483 (1996).

<sup>14</sup>S. S. Eaton, J. Harbridge, G. A. Rinard, G. R. Eaton, and R. T. Weber, *Appl. Magn. Reson.* **20**, 151 (2001).

<sup>15</sup>L. K. Aminov, I. N. Kurkin, S. P. Kurzin, D. A. Lukoyanov, I. Kh. Salikhov, and R. M. Rakhmatullin, *JETP* **84**, 183 (1997).

<sup>16</sup>H. Haeuseler and G. Haxhillazi, *J. Raman Spectrosc.* **34**, 339 (2003).

<sup>17</sup>I. M. Brown, *J. Chem. Phys.* **60**, 4930 (1974).

<sup>18</sup>I. M. Brown, *J. Chem. Phys.* **65**, 630 (1976).

<sup>19</sup>A. E. Stillman, L. J. Schwartz, and J. H. Freed, *J. Chem. Phys.* **73**, 3502 (1980).

<sup>20</sup>K. Nakagawa, M. B. Candelaria, W. W. C. Chik, S. S. Eaton, and G. R. Eaton, *J. Magn. Reson.* (1969-1992) **98**, 81 (1992), and references therein.

<sup>21</sup>M. T. Bennebroek and J. Schmidt, *J. Magn. Reson.* **128**, 199 (1997).

<sup>22</sup>B. Epel, A. Pöpl, P. Manikandan, S. Vega, and D. Goldfarb, *J. Magn. Reson.* **148**, 388 (2001).

<sup>23</sup>J. van Tol, L. C. Brunel, and P. Wyder, *Bull. Am. Phys. Soc.* **44** (1), 1130 (1999).

<sup>24</sup>S. Li and J. F. Clauser, *Phys. Rev. A* **49**, 2702 (1994).

<sup>25</sup>J. R. Morton and K. F. Preston, *J. Magn. Reson.* (1969-1992) **30**, 577 (1978).